

REFINED MEASUREMENT AND VALIDATION OF PERFORMANCE AND LOADS OF A MACH-SCALED ROTOR AT HIGH ADVANCE RATIOS

Lauren Trollinger
trollinger.lauren@gmail.com
Graduate Research Assistant

Xing Wang
wxing99@umd.edu
Graduate Research Assistant

Inderjit Chopra
chopra@umd.edu
Distinguished University Professor

Alfred Gessow Rotorcraft Center
Dept. of Aerospace Engineering, University of Maryland
College Park, MD, 20742, USA

Slowed-rotor compound helicopters support high speed flight by reducing the main rotor RPM as cruise speed increases to maintain sub-critical tip Mach numbers on the advancing side, resulting in high advance ratio (μ) flight regimes. This work investigates the performance and vibratory loads of a Mach-scale rotor with highly similar, non-instrumented blades (untwisted, untapered) at advance ratios up to 0.9. A 4-bladed, articulated rotor with a diameter of 5.6 ft. was tested in the Glenn L. Martin Wind Tunnel at 30%, 40%, and 50% of nominal speed (corresponding to advancing tip Mach numbers up to 0.53). For each test point, the rotor is trimmed to minimize cyclic flap angles. Collective sweeps from -2° to 12° were performed for each flight condition and longitudinal shaft tilt angles of -4° , 0° , and 4° (positive aft) were tested. Blade root pitch and flap motion, trim cyclics, shaft power, and steady and vibratory hub loads were measured. Blade similarity was shown to improve rotor track and trim at high μ . Thrust reversal was observed at an advance ratio of 0.9, but positive shaft tilt increased lift, and overall performance at high μ . Vibratory hub loads are shown to increase with advance ratio. Correlations of the measured data with predictions from the comprehensive analysis code UMARC are presented, and show satisfactory agreement for rotor performance over the entire range of advance ratios.

NOMENCLATURE

C_D	rotor drag coefficient
C_{De}	equivalent rotor drag coefficient
C_T	rotor thrust coefficient
C_P	shaft power coefficient
c	local blade chord, 3.15 in.
L/D_e	rotor lift-to-drag ratio
P	frequency per revolution, n/rev
R	rotor radius, 2.78 ft.
RPM	revolutions per minute
α_S	shaft tilt angle (positive aft)
γ	Lock number, $\rho ac R^4 / I_b$
θ_0	collective pitch
θ_{1c}	lateral cyclic
θ_{1s}	longitudinal cyclic
μ	advance ratio, $V_\infty / \Omega R$
σ	rotor solidity, 0.1196

1. INTRODUCTION

The objective of this work is to build upon the existing understanding of the aeromechanics of a rotor in the high advance ratio flight regime by first obtaining refined experimental measurements of a slowed rotor at high advance ratios, then using the

experimental test data to validate the predictive capabilities of UMARC, an in-house comprehensive analysis tool.

Over the last few years, there has been an industry-wide push for high speed rotorcraft capable of efficient cruise between 300 and 400 knots [1]. Traditionally, the high speed flight envelope of conventional helicopters with edgewise rotors has been limited by compressibility effects on the advancing side as well as reverse flow and dynamic stall on the retreating side. Slowing the rotor can minimize these compressibility effects and decrease the profile power, but also results in high advance ratio flight that can cause loss of lift on the retreating side and high vibratory loads. Reducing the rotor tip speed in forward flight is a viable method of extending the cruise speed of a helicopter, but the aeromechanics of the rotor in high advance ratio flight regimes must be understood. A slowed rotor with uniform, highly similar blades was tested in the University of Maryland Glenn L. Martin Wind Tunnel (GLMWT), and the measured data was used to validate an in-house predictive model.

Historically, there have been five major wind tunnel experiments on slowed rotors at high advance ratios. In 1933, an isolated Pitcairn PCA-2 autogiro rotor was tested to an advance ratio of 0.7, demonstrating

a maximum achievable lift-to-drag ratio of 7.0 at $\mu = 0.35$ [2]. Jenkins [3] tested a two-bladed, 15-foot-diameter teetering rotor with an untwisted, untapered NACA 0012 airfoil to $\mu = 1.45$, providing the first published evidence of thrust reversal. Later experiments included an H-34 articulated rotor [4] and a UH-1D teetering rotor [5], both of which were tested at high μ in the NASA Ames 40 by 80 ft. wind tunnel. These first four tests provided only performance measurements, blade root motions, and some flow visualization, with no detailed set of rotor properties. Several authors [4, 6, 7, 8] compared these experimental data sets with state-of-the-art predictive models of the time, but the measurements were not detailed enough to resolve the discrepancies in the predictive results.

Datta, Yeo, and Norman [9] reported the test results of a full-scale UH-60A rotor up to $\mu = 1.0$ in the NASA Ames large-scale wind tunnel in an attempt to provide a high quality, comprehensive data set that would identify the sources of discrepancies in analytical models. The blade properties are publicly available, and the blades were instrumented with pressure sensors to measure airloads as well as strain gauges and accelerometers to measure structural blade loads. Performance data, vibratory loads, and rotor wake were measured. Thrust reversal was observed between μ of 0.9 to 1.0, and rearward longitudinal shaft tilt improved the rotor lift-to-drag ratio. Reverse chord dynamic stall was evidenced by the pressure measurements on the suction side of the blade in the reverse flow region. An evaluation of the measured data was performed by Potsdam et al. [10] using coupled Helios/RCAS CFD-CSD analysis, and demonstrated good correlation for sectional airloads, trim cyclics, and rotor performance when blade shank drag corrections were included.

Previous work by researchers at the University of Maryland has provided detailed performance data, vibratory loads, and blade loads measurements for instrumented rotor blades at high advance ratios [11, 12] with a maximum advancing tip Mach number of 0.45. Berry and Chopra [12, 13] summarized the results of five slowed rotor tests (operating at primarily 30% of nominal rotor speed, NR) performed in the GLMWT up to advance ratios of 1.61, noting that thrust reversal occurred between advance ratios of 0.8 and 0.9 regardless of twist, camber, or airfoil profile. Evidence of reverse chord dynamic stall was observed in the blade torsion and pitch link loads, and an increase in performance and vibratory loads occurred with increasing advance ratio. The experimental data was evaluated with an in-house

comprehensive analysis tool, UMARC, by Bowen-Davies and Chopra [14, 15]. Wang, Saxena, and Chopra [11] utilized the same instrumented rotor to expand the flight envelope of the previous tests, operating primarily at 40% NR and achieving advance ratios up to 0.8. Difficulties in trimming and tracking the rotor at higher advance ratios were attributed to dissimilarity in the blades, likely caused by the incorporation of sensors into the blade structure. Both tests reported rotor properties, including blade geometry, stiffnesses, and inertial distribution, and the blades were instrumented with pressure sensors and strain gauges to measure sectional airloads and structural loads. Rotor performance and vibratory loads, blade root flap angles, and control cyclics were also measured. Wang et al. correlated the test data to predictions from UMARC, and showed well-matched control angles as well as good agreement in rotor performance; however, the correlations tended to degrade at high advance ratios.

The present work investigates the performance and vibratory loads of a Mach-scaled rotor slowed to achieve advance ratios up to 0.9. This investigation aims to mitigate the difficulty in tracking and trimming rotors at high advance ratios by improving blade similarity and collecting direct pitch measurements, both of which are key to reliable baseline performance data for correlation studies. The data set is used to correlate rotor performance, vibratory loads, and control angles using UMARC comprehensive analysis.

2. EXPERIMENTAL TEST SETUP

All tests utilized the facilities and equipment housed within the Alfred Gessow Rotorcraft Center (AGRC), which included an articulated rotor test stand, hover tower, and data acquisition system as well as the

Table 1. UMD rotor properties.

Parameter	Value
No. of blades	4
Blade profile	NACA 0012
Blade radius, in. (m)	33.5 (0.843)
Blade chord, in. (m)	3.15 (0.080)
Nominal rotor RPM	2300
Lock no.	4.96
Tip Mach no.	0.60
Hinge offset	6.3%
Root cutout	16.4%

University of Maryland's Glenn L. Martin Wind Tunnel (GLMWT). A simplified fuselage was mounted to the rotor rig, as shown in Figure 1.

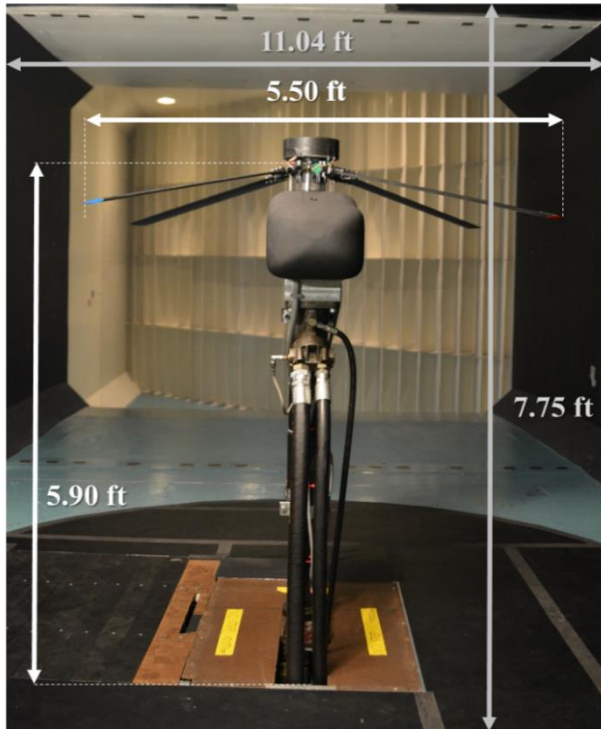


Figure 1. Rotor test stand installed in the Glenn L. Martin Wind Tunnel test section.

Initial wind tunnel tests were performed in October 2016, followed by more refined tests in February 2017. A 4-bladed, fully articulated rotor with a radius of 33.5 in. and chord of 3.15 in. ($\sigma = 0.120$) was used for both tests. The NACA 0012 blades were untwisted and untapered, with a hinge offset of 6.4%R, a root cutout at 16.4%R, and a nominal angular velocity of 2300 RPM. The 2016 blades ($\gamma = 4.83$) were instrumented, making them slightly heavier than the non-instrumented blades ($\gamma = 4.96$) used in the 2017 tests. Additionally, higher rotor RPM settings were used to achieve an advancing tip Mach number of 0.53, closer to the design tip Mach of 0.60, and to provide better correlation of rotor drag. During construction of the latter rotor model, great care was taken to build structurally and aerodynamically similar blades.

Fixed-frame sensors included a 3-component accelerometer, a 5-component hub balance, and a torque sensor on the rotor shaft for torque measurement. Linear Variable Displacement Transducer (LVDT) sensors monitored swashplate displacement and provided control angles, while a

shaft encoder monitored rotor RPM. Hall effect sensors measured flap angles, and strain gauges recorded pitch link loads. The blades from the 2016 test were instrumented with fourteen Endevco pressure sensors, which were embedded at 30% radius in blades 1 and 3, and bending and torsional strain gauges, which were surface-bonded to blades 2 and 4. While valuable findings were obtained from the instrumented blades during the 2016 test, dissimilarities in blade construction led to large differences in respective blade motions at high advance ratios.

In 2017, non-instrumented blades were used to preserve blade similarity and maintain structural uniformity along the blade span. Incorporating sensors into the blade structure inherently affected the blade's internal characteristics; the sensor section of the 2016 blades introduced up to 5% variation in structural and inertial characteristics among the four blades. Therefore, benchmark wind

Table 2. Non-instrumented blade properties.

	Blade 1	Blade 2	Blade 3	Blade 4	Variance (%)
Mass (g)	197.4	197.5	197.4	197.3	0.05
I_B (kg-m ²)	0.0578	0.0592	0.0587	0.0592	0.84
f_n (Hz)	13.5	13.4	13.0	13.0	2.08
EI (Nm ²)	29.3	30.8	30.8	29.4	2.53
GJ (Nm ² /rad)	23.3	23.7	23.5	23.8	0.95

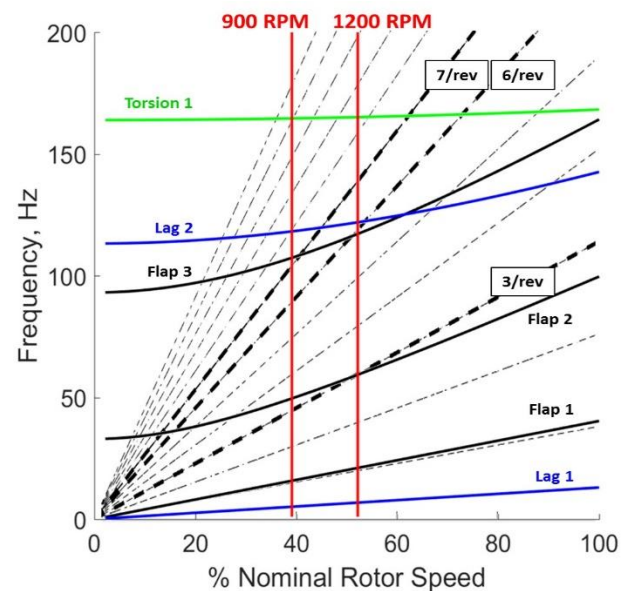
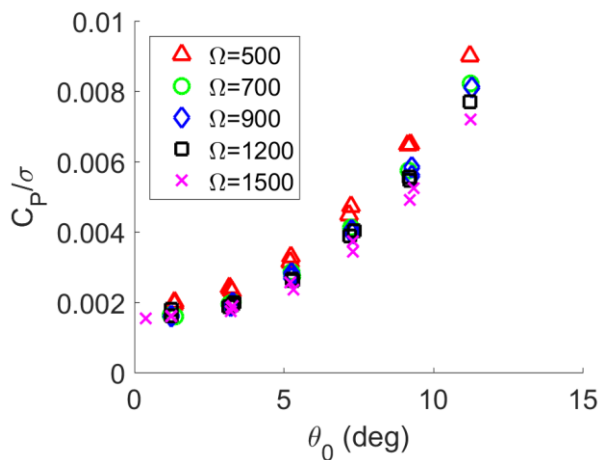


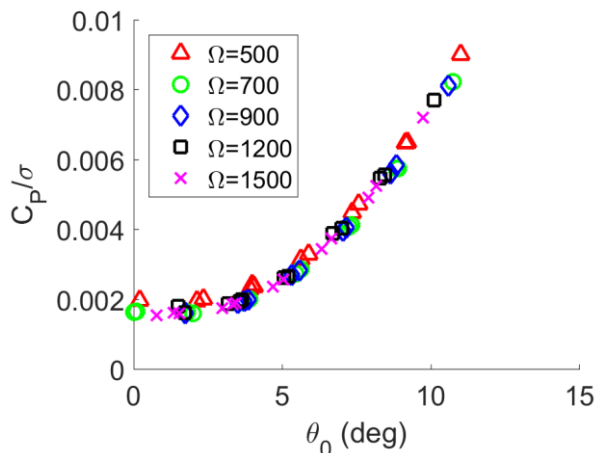
Figure 2. Calculated fan plot for multiple rotor speeds, with operational RPMs marked in red.

tunnel tests were carried out in 2017 with four non-instrumented rotor blades. To ensure sufficient similarity in the set of blades, extensive structural testing was performed to quantify blade characteristics; measurements of blade mass, flap inertia, frequency response, and bending and torsional stiffnesses were carried out. The final blade set demonstrated a maximum variance of 2.5%, one-half the degree of dissimilarity of the 2016 test. The blade properties shown in Table 2 were used to calculate the rotor fan plot shown in Fig. 2, where the operational rotor RPMs are highlighted in red.

Additional Hall effect sensors were installed on the hub for the 2017 tests to supplement the swashplate



(a) Input collective settings measured by fixed-frame LVDT sensors on the swashplate.



(b) Actual collective angles measured by Hall effect sensors on each blade grip.

Figure 3. Direct pitch measurement at the blade root provides higher-accuracy data set.

measurements by measuring the root pitch of each blade directly. Because of the control system stiffness of the hub and swashplate linkages, small discrepancies exist between the control inputs from the swashplate measurements and the actual blade pitch. The Hall effect sensing of blade root pitch notably improved accuracy in collective measurements, as shown in Fig. 3.

3. UMARC MODELING

The University of Maryland Advanced Rotorcraft Code, UMARC [14, 16], is a comprehensive analysis tool used to calculate the aeromechanics of a rotor in high advance ratio environments. UMARC is a finite element discretization in space and time that uses a lifting-line approach and NACA 0012 airfoil table look-ups for sectional lift, drag, and pitching moment coefficients. The model uses 12 time elements and 20 spatial elements; each with 15 degrees of freedom (Table 3). To simplify the computations, modal reduction (10 modes) is used.

Derived from Hamilton's principle, the analysis includes coupled elastic flap, lag, twist, and axial deformations to second order precision [17]. UMARC utilizes the Weissinger-L trailed wake model for predicting nearwake up to 30° after each blade, and incorporates far wake using the Bagai-Leishman relaxation free wake model [18]. The Leishman-Beddoes attached unsteady [19] and dynamic stall [20] models are used to predict the unsteady flow in the shed wake.

Table 3. UMARC baseline model

Parameter	Description
No. time elements	10
No. spatial elements	20
Nearwake	Weissinger-L model trailing 30° after the blade
Farwake	Bhagwat-Leishman model
Tip trailers	Single trailer
Root trailers	For vibratory predictions only
Blade shank correction	None
Fuselage model	None

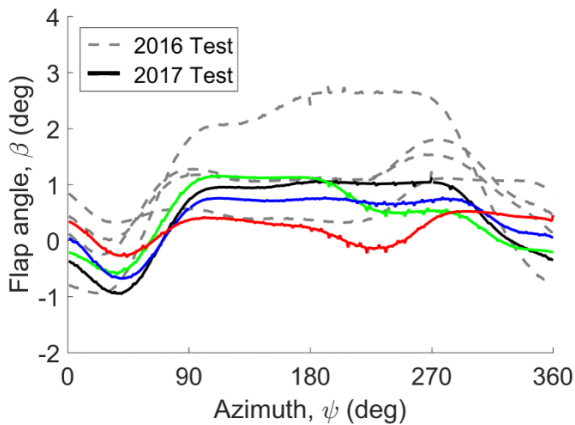
This analysis models an untwisted, constant-chord blade with a NACA 0012 profile. It does not account for a fuselage, corrections to root shank drag (tared out during wind tunnel testing), or a wake trailer at the blade root. All cases were trimmed to zero first harmonic flapping for fixed collective angles.

4. RESULTS

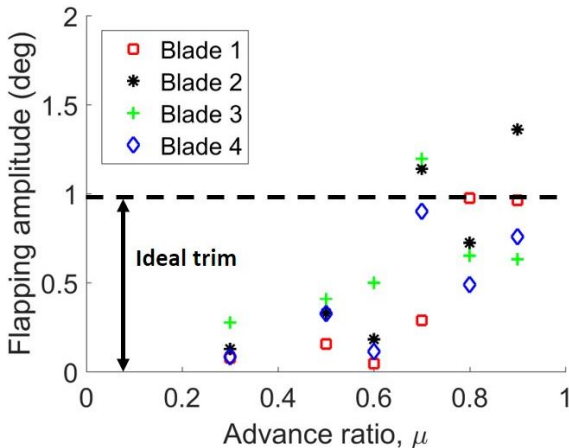
Collective pitch sweeps were performed for advance ratios up to 0.9, and the effects of shaft tilt were explored at the highest μ . Collectively, this work provides refined test data and analysis for a Mach-scale rotor operating at high advance ratios for validation of comprehensive analysis predictions and provides insights into aeromechanic phenomena to support the development of future high speed rotorcraft.

4.1 Track and Trim

The 2016 test carried out collective sweeps up to $\mu = 0.7$ at 900 RPM. Though a consistent trim state was achieved at these advance ratios, the blade tip path tracking became problematic at higher wind tunnel speeds. The primary goal of the 2017 test was to achieve refined high advance ratio performance



(a) Phase-averaged flapping amplitudes of all four blades at $\mu = 0.7$.

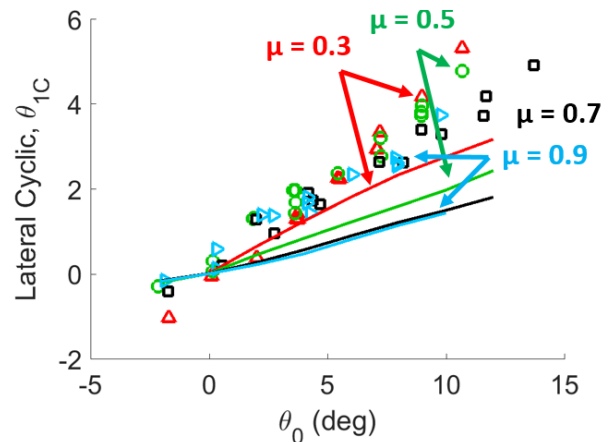


(b) The rotor was trimmed to within 1° of zero flapping amplitude for most advance ratios.

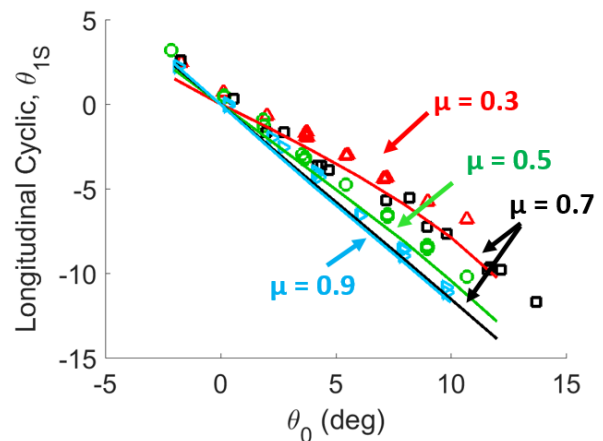
Figure 4. Rotor track and trim at 900 RPM. Blade 1 was used as a reference.

measurements while maintaining a reliable track and trim state. Non-instrumented blades and direct pitch measurements helped to minimize the tracking problem, reducing the maximum peak-to-peak flapping by 30% at an advance ratio of 0.7 (Fig. 4a). All cases were trimmed to zero first harmonic flapping within a tolerance of 1° . The flapping amplitude of Blade 1 was used as a reference. Despite instabilities experienced at $\mu = 0.9$, the rotor stayed well within a half-degree of the trim tolerance for the full range of advance ratios tested (Fig. 4b).

The lateral (θ_{1C}) and longitudinal (θ_{1S}) trim cyclics



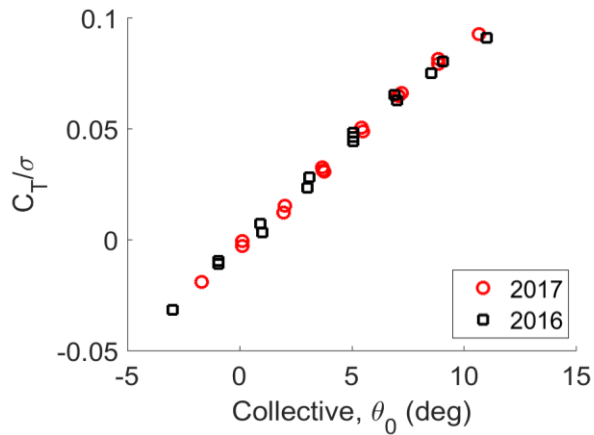
(a) Lateral trim cyclic versus collective



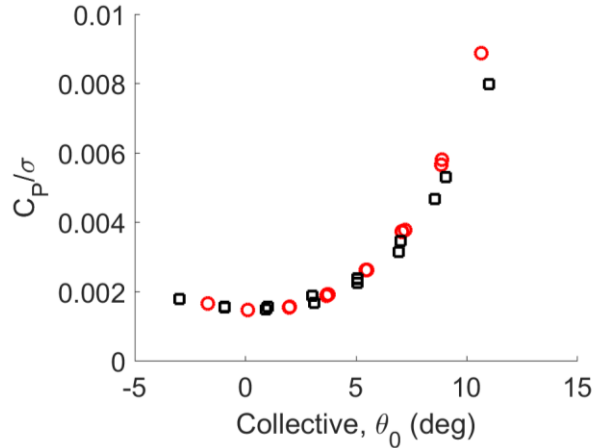
(b) Longitudinal trim cyclic versus collective

Figure 5. Trim cyclics versus collective for select advance ratios up to 0.9 and 900 RPM.

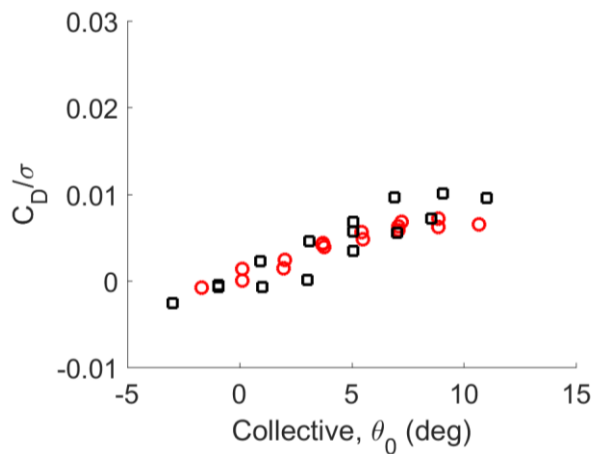
(symbols) are shown in Fig. 5 for select advance ratios, and the UMARC predictions (lines) show acceptable agreement in the trends and magnitudes with an offset of up to 2° . A slightly steeper slope in the lateral cyclic measurements is likely due to the



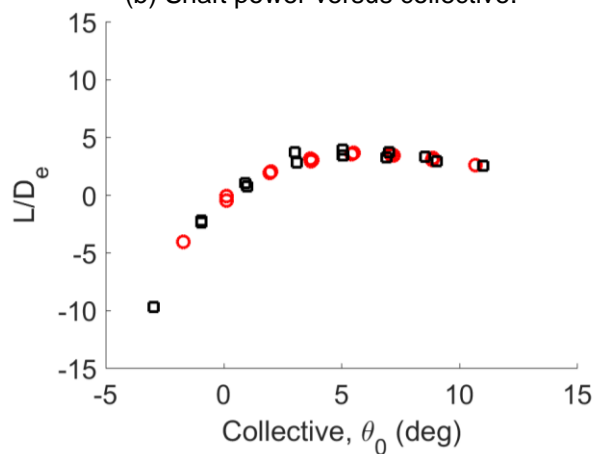
(a) Lift coefficient versus collective.



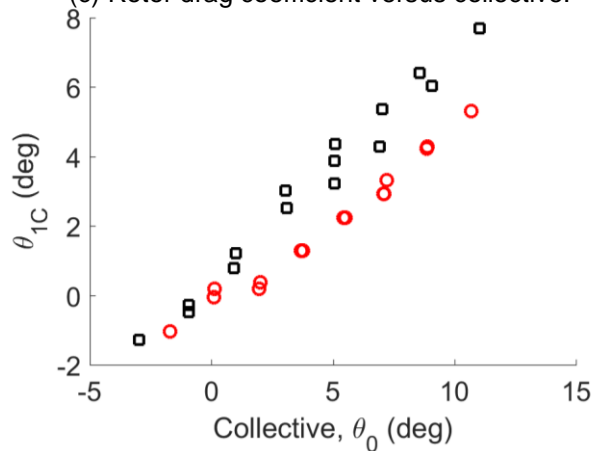
(b) Shaft power versus collective.



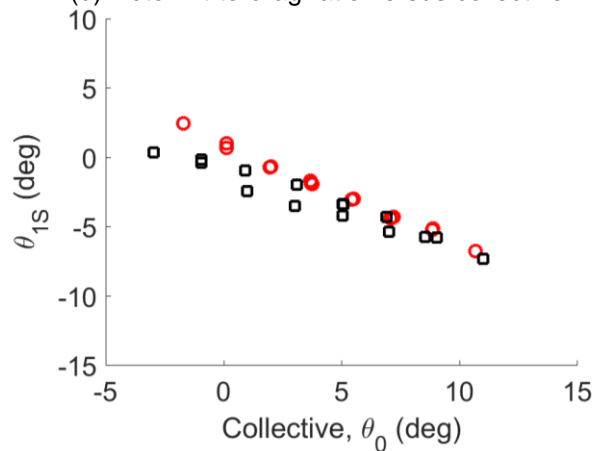
(c) Rotor drag coefficient versus collective.



(d) Rotor lift-to-drag ratio versus collective.

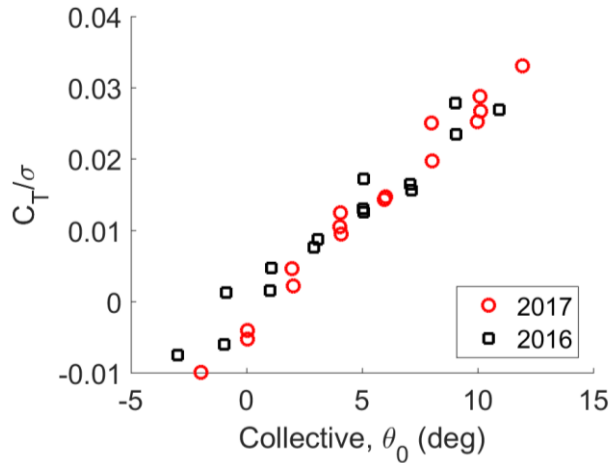


(e) Lateral cyclic versus collective.

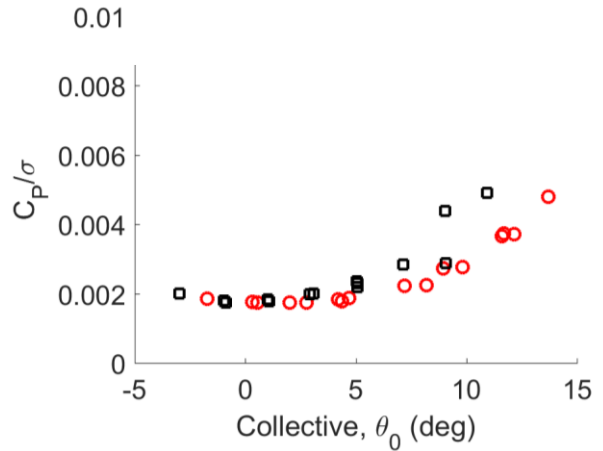


(f) Longitudinal cyclic versus collective.

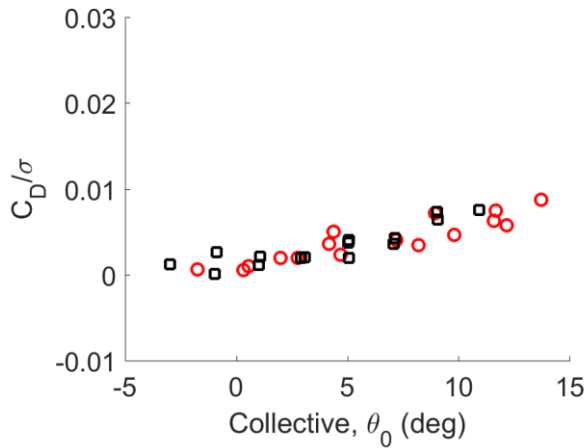
Figure 6. Comparison of 2016 test with instrumented blades (5% variance) to 2017 test with non-instrumented, highly similar blades (2.5% variance), direct pitch measurement, and a simplified fuselage. The instrumented blades were slightly heavier, and thus required slightly greater shaft torque. Performance data shows consistent agreement between the two tests (900 RPM, $\mu = 0.3$).



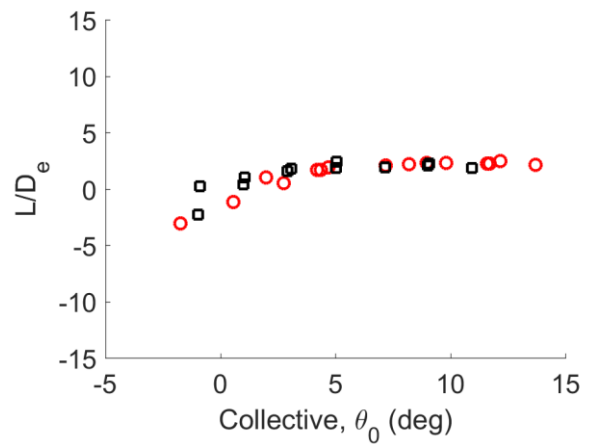
(a) Lift coefficient versus collective.



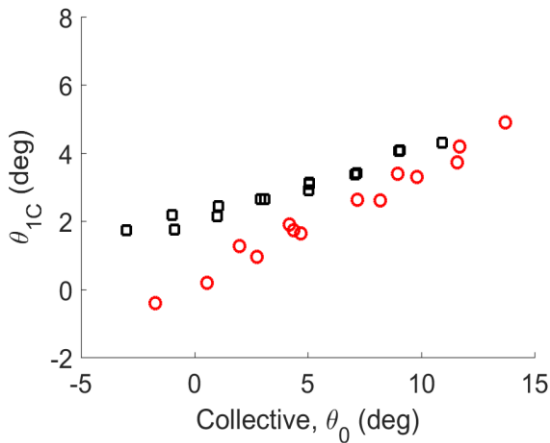
(b) Shaft power versus collective.



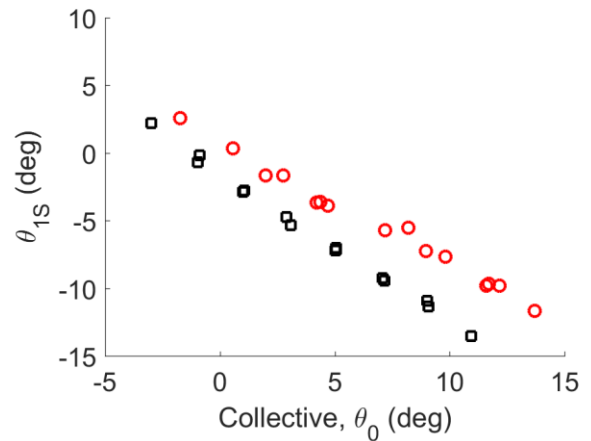
(c) Rotor drag coefficient versus collective.



(d) Rotor lift-to-drag ratio versus collective.



(e) Lateral cyclic versus collective.



(f) Longitudinal cyclic versus collective.

Figure 7. Comparison of 2016 test with instrumented blades (5% variance) to 2017 test with non-instrumented, highly similar blades (2.5% variance), direct pitch measurement, and a simplified fuselage. The instrumented blades were slightly heavier, and thus required slightly greater shaft torque. Performance data shows consistent agreement between the two tests (900 RPM, $\mu = 0.7$).

presence of the fuselage, which was not modeled in the analysis. Upwash caused by the nose of the fuselage affects the front of the rotor disk, requiring more lateral cyclic to trim the rotor.

The effects of blade similarity and direct pitch measurement are shown in Figures 6 and 7. The consistency of the results, from both the 2016 tests with instrumented blades and the 2017 tests with non-instrumented blades, serves to demonstrate that rotor performance measurements were largely unaffected by the 2-5% dissimilarity in the blade characteristics. The difference in trim cyclics, particularly lateral cyclic, were affected by the presence of a simplified fuselage in the 2017 tests.

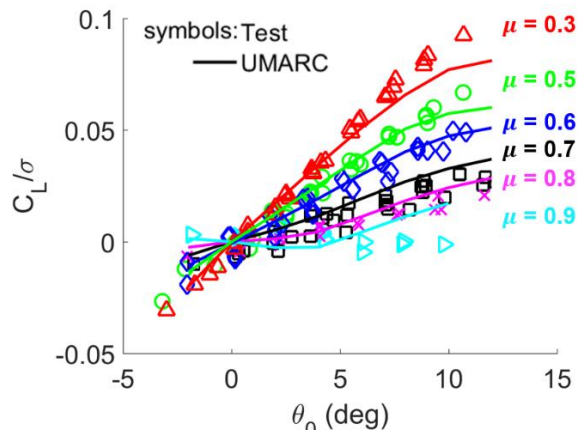
4.2 Rotor Performance

Figure 8 shows the validation of lift and shaft power versus collective for advance ratios from 0.3 to 0.9. The trends are well captured for all advance ratios. Differences in the magnitude of lift coefficient (Fig. 8a) near $\theta_0 = 10^\circ$ at low advance ratios likely indicate the premature onset of stall in the analysis. At $\mu = 0.9$, the lift is slightly over-predicted for the highest collective angles.

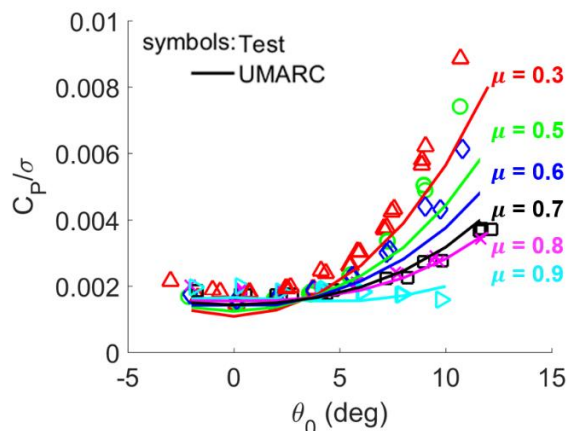
Overall, the slopes and magnitudes of lift to collective are well captured, demonstrating the decreasing sensitivity to collective as advance ratio increases. This decrease in slope with increasing advance ratio occurs as the reverse flow region on the retreating side of the rotor grows. In reverse flow, the geometric trailing edge of the blade becomes the aerodynamic leading edge with a negative angle of incidence; therefore, the blade produces less thrust with increased collective inputs. At $\mu = 0.9$, the net thrust begins to decrease with higher collectives. This phenomenon, called thrust-collective control reversal, occurs when the negative lift on the retreating side grows too large to be balanced out by the advancing side, and the rotor can only be trimmed by producing net negative lift.

The predictions for shaft torque coefficient (Fig. 8b) agree satisfactorily well with the measured data at high advance ratios, though the power is slightly under-predicted at higher collectives for $\mu \leq 0.6$. At $\mu = 0.9$, the shaft power is no longer affected by changes in collective. The decrease in required power is due to the increasing drag on the blade in

reverse flow, which accelerates the rotor on the retreating side. The drag of the rotor, shown in



(a) Rotor lift coefficient versus collective.



(b) Shaft power coefficient versus collective.

Figure 8. Rotor lift and shaft power coefficients for increasing advance ratios at 900 RPM and 1200 RPM; $\alpha_s = 0^\circ$.

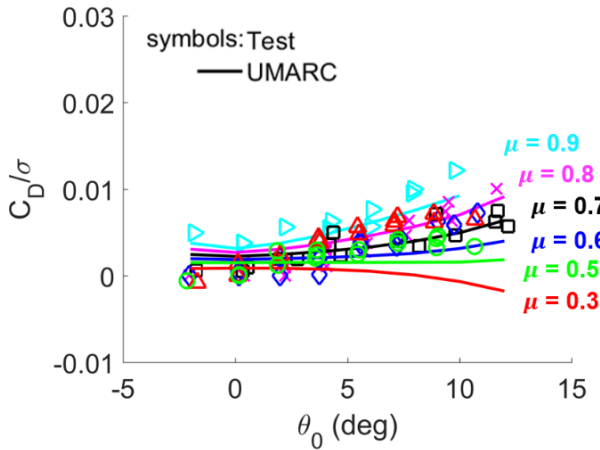
Fig. 9a, was isolated from the drag due to the test stand and hub by taring the rotor at each flight condition. Blade shanks were used during the tare test to accurately account for hub drag. The correlations are very good at advance ratios above $\mu = 0.5$, and the analysis captures the overall magnitudes as well as the increase in drag with increasing collective. At the lowest advance ratio of 0.3, the prediction correlates well at low collectives, but underestimates the magnitudes at higher collectives. In general, the drag is near zero at $\theta_0 = 0^\circ$, and increases with positive collective angles. The freestream velocity is sufficiently high at

$\mu = 0.9$ that drag increases with negative collectives as well.

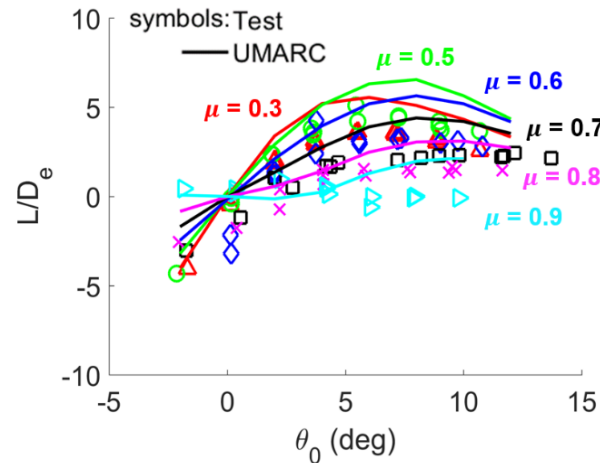
A key measure of the performance of a rotor is its effective lift-to-drag ratio, which is defined in Eq. 1.

$$\frac{L}{D_e} = \frac{C_L}{C_D + \frac{C_P}{\mu}} \quad (1)$$

The variation of effective lift-to-drag ratio with collective is presented in Fig. 9b and shows good correlation with UMARC predictions. Good agreement in rotor lift and power, both of which are of larger magnitudes than rotor drag, results in well-predicted lift-to-drag across the range of advance ratios. A small over-prediction at higher collective



(a) Rotor drag coefficient versus collective.



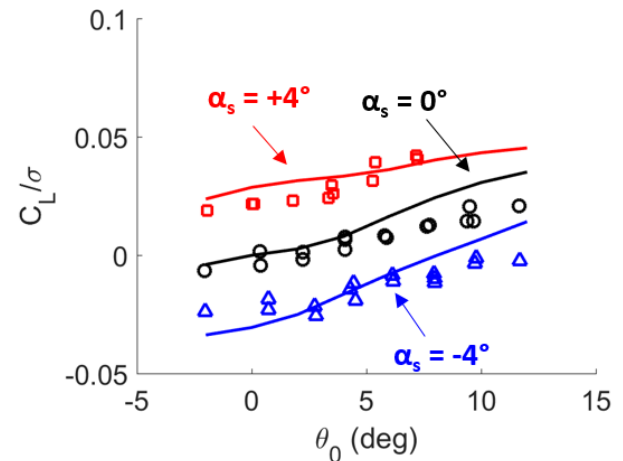
(b) Rotor lift-to-drag ratio versus collective.

Figure 9. Rotor drag coefficient and lift-to-drag ratio for increasing advance ratios at 900 RPM and 1200 RPM; $\alpha_s = 0^\circ$.

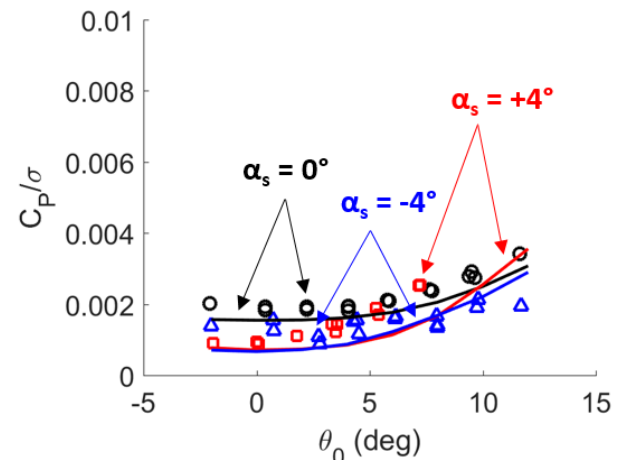
angles is the combined result of slight over-predictions in lift and under-predictions in power, which increases overall L/D_e . The general trends are well captured, and the lift-to-drag ratio becomes less sensitive to changes in collective as the advance ratio increases. At $\mu = 0.9$, there is no longer any change with collective. Overall, the rotor lift-to-drag is well captured for the full range of advance ratios for 900 RPM (Fig. 9b) and 1200 RPM (not shown).

4.3 Effect of Shaft Tilt

The 2016 results showed a slight rearward shaft tilt ($\alpha_s = +2^\circ$) increased the lift-to-drag ratio, so a wider shaft tilt test envelope was included in the 2017 tests ($-4 \leq \alpha_s \leq +4^\circ$) for advance ratios from 0.5 to 0.8 at 900 RPM and 0.5 to 0.7 at 1200 RPM. Figure 10 shows the variation of rotor lift and torque from



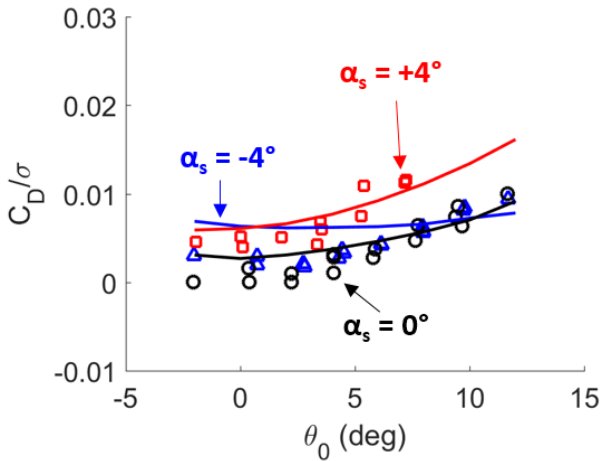
(a) Lift versus collective.



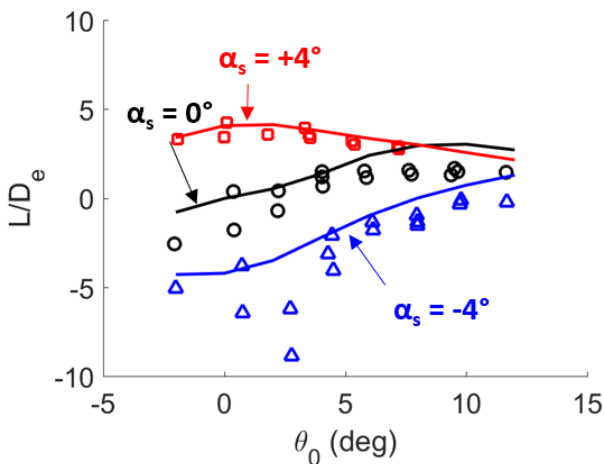
(b) Shaft power coefficient versus collective.

Figure 10. Effect of aft shaft tilt ($+4^\circ$) and forward shaft tilt (-4°). Data shown is for $\mu = 0.8$ and 900 RPM.

experiment (marked with symbols) and analysis (marked by lines) for $\mu = 0.8$. Positive (aft) shaft tilt significantly increases rotor lift coefficient and decreases shaft power at low collectives.



(a) Rotor drag coefficient versus collective.



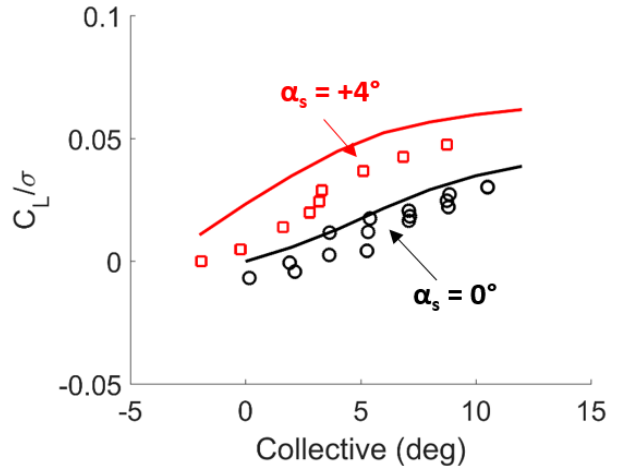
(b) Effective lift-to-drag versus collective.

Figure 11. Effect of aft shaft tilt (+4°) and forward shaft tilt (-4°) on drag and lift-to-drag ratio. Data shown is for $\mu = 0.8$ and 900 RPM.

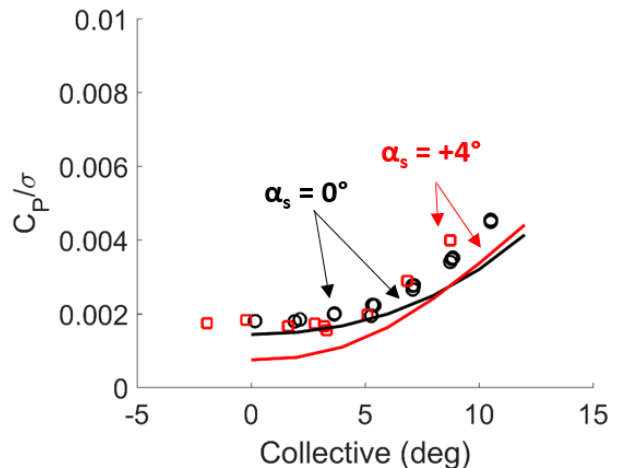
Figure 10 shows that +4° shaft tilt generates significantly greater thrust while shaft torque is slightly decreased for low collectives. The correlations for rotor drag coefficient are shown in Fig. 11a; aft and zero shaft tilt are especially well predicted. The drag increases with nonzero shaft tilt, but the magnitude is small in comparison to lift and torque. Thus, effective lift-to-drag (Fig. 11b) increases with positive (aft) shaft tilt. The UMARC simulations show good agreement with the

measured data, and the analysis captures both the trends and the magnitudes well.

Similar trends are seen at 1200 RPM and an advance ratio of 0.7, as shown in Figure 12. Aft shaft tilt was compared to zero shaft tilt at this condition; forward shaft tilt was not tested due to limited time in the wind tunnel. The lift coefficient (Fig. 12a) once again visibly increases with aft shaft tilt, while the



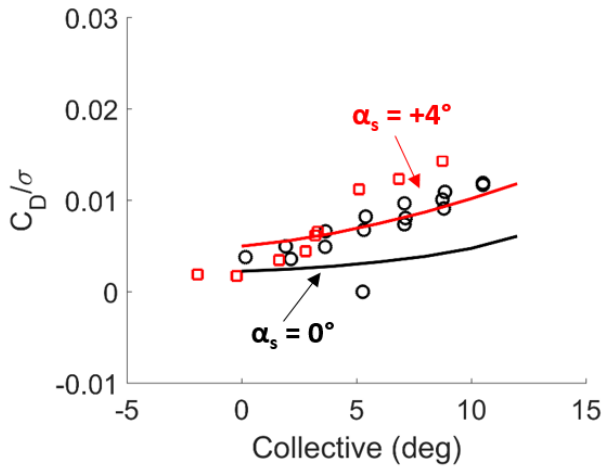
(a) Positive (aft) shaft tilt significantly increases rotor lift coefficient.



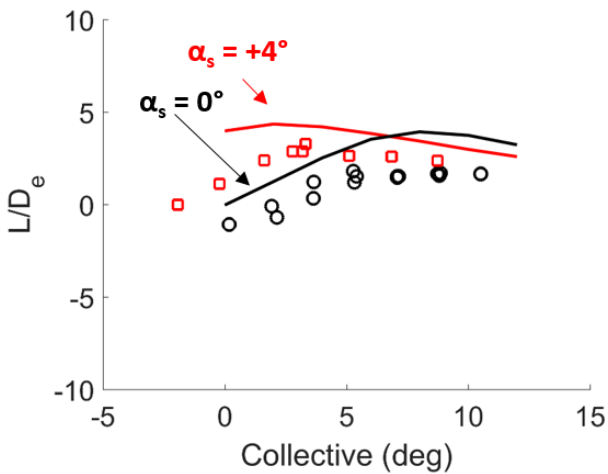
(b) Shaft tilt does not have a significant effect on the power coefficient at low collectives.

Figure 12. Effect of aft shaft tilt (+4°) on rotor lift and shaft torque coefficients. Data shown is for $\mu = 0.7$ and 1200 RPM.

shaft torque coefficient (Fig. 12b) is not significantly affected and is only slightly increased at high collective angles. The rotor drag (Fig. 13a) shows trends similar to the 900 RPM data, demonstrating higher drag with aft shaft tilt.



(a) Rotor drag coefficient versus collective.



(b) Effective lift-to-drag ratio versus collective.

Figure 13. Effect of aft shaft tilt (+4°) on rotor drag and lift-to-drag ratio. Data shown is for $\mu = 0.7$ and 1200 RPM.

However, there is a more pronounced offset between the experimental and predicted results for the data at 1200 RPM than the results at 900 RPM, which may reflect less accurate drag predictions at higher Mach numbers. The effective lift-to-drag ratio shown in Fig. 13b once again increases with aft shaft tilt, but shows less of an overall increase than the results at 900 RPM.

4.3 Vibratory Loads

The vibratory hub loads were measured and the harmonics were extracted. The 4/rev (4P) component of the vertical force is shown in Fig. 14, and clearly increases in both slope and magnitude as advance ratio increases. At low μ , the 4P component is less affected by changes in collective;

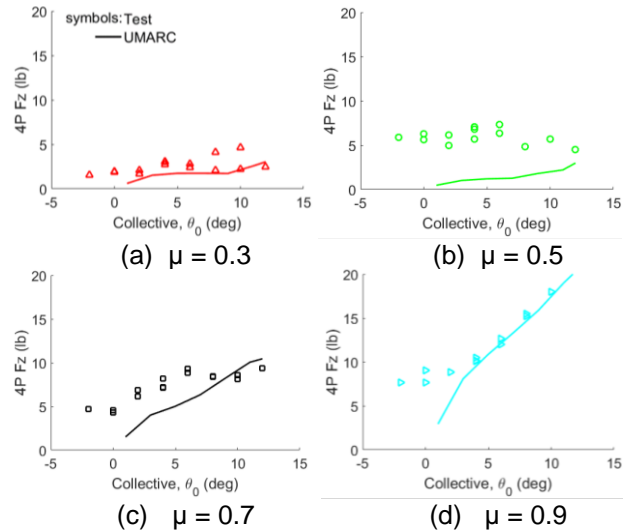


Figure 14. The 4/rev vertical force for the 2017 test with a fuselage. Data shown is for select advance ratios at 900 RPM and $\alpha_s = 0^\circ$.

however, at higher μ the 4P component increases more sharply. Experimental results for $\mu = 0.7$ and $\mu = 0.9$ indicate a minimum value occurs near 0° collective, as theory would suggest. UMARC captures the trends, demonstrating an overall increase in the slope of the 4/rev components with

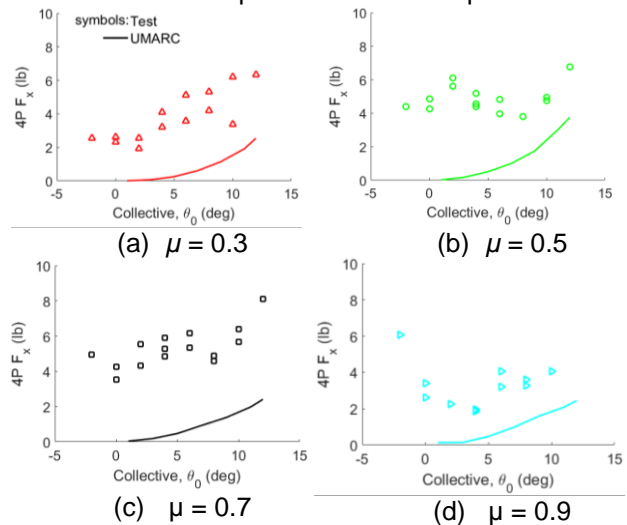


Figure 15. The 4/rev propulsive force for the 2016 test with a fuselage. Data shown is for select advance ratios at 900 RPM and $\alpha_s = 0^\circ$.

increasing advance ratio. The magnitudes appear to be better predicted at low μ when unsteady effects are small, while at higher μ the inclusion of additional inboard trailers in the analysis provide better correlation.

The 4/rev component of the propulsive force is shown in Fig. 15. The predictions from UMARC analysis capture the increase in vibration as collective increases, the magnitudes are under-predicted. An increase in magnitude with advance ratio is evident for lower to moderately high advance ratios; however, the vibration at $\mu = 0.9$ is significantly reduced. This is also evident in Fig. 16, which shows the hub load harmonics for the in-plane and vertical forces for the range of advance ratios tested. The vibratory loads increase with advance ratio, though the in-plane forces decrease abruptly at an advance ratio of $\mu = 0.8$. The large 1P component present in both loads indicates an imbalance in the rotor and hub; the variation with advance ratio in the vertical force suggests an aerodynamic dependence, while the independence of the in-plane forces suggest a mass imbalance.

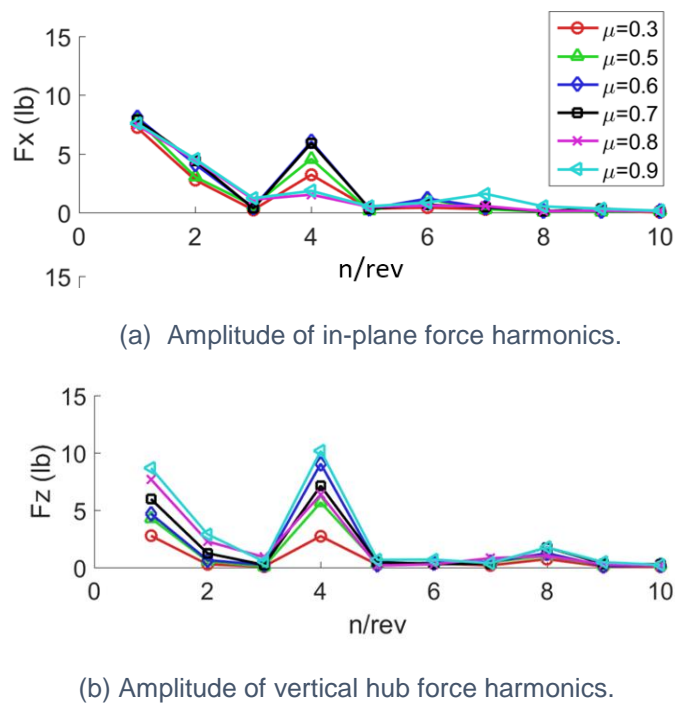


Figure 16. Harmonics of the in-plane and vertical hub loads for 900 RPM and $\alpha_s = 0^\circ$.

The vibratory loads of the 2017 test with a fuselage were compared to the 2016 test without a fuselage, and the 4P vertical and propulsive forces are shown in Figures 17 and 18, respectively. While the 2017 test achieved advance ratios up to 0.9 at 900 RPM, the 2016 test did not due to difficulties trimming the rotor; this is reflected in the data shown in Figures 17 and 18. The presence of the fuselage, combined with the slight dissimilarities in the two blade sets, shows slight differences in the 4P vertical forces such that

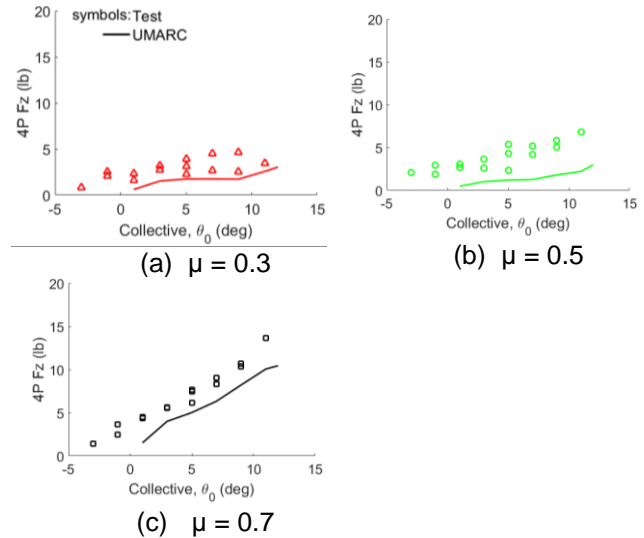


Figure 17. The 4/rev vertical force for the 2016 test without a fuselage. Data shown is for $0.3 < \mu < 0.7$ at 900 RPM and $\alpha_s = 0^\circ$.

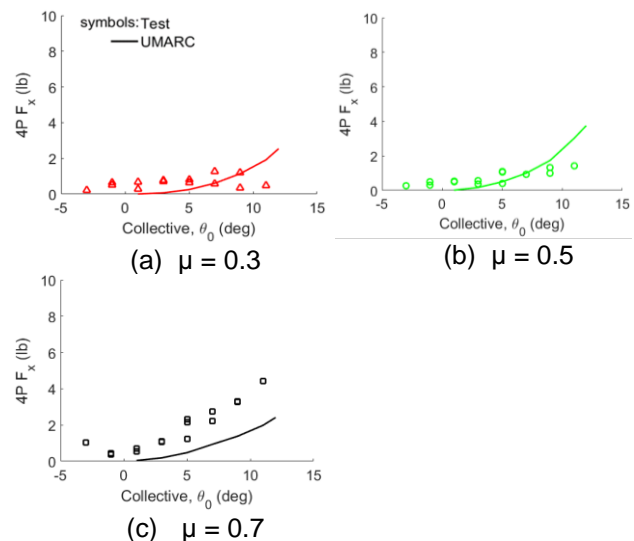


Figure 18. The 4/rev propulsive force for the 2016 test without a fuselage. Data shown is for $0.3 < \mu < 0.7$ at 900 RPM and $\alpha_s = 0^\circ$.

the 2016 test with no fuselage (shown in Fig. 17) better matches the slopes and magnitudes of the predicted results for all advance ratios shown. The 4P propulsive forces (shown in Fig. 18) show a more significant difference between the two tests, implying the presence of the fuselage had a larger impact on the in-plane vibration of the 2017 wind tunnel tests.

CONCLUSIONS

This research effort experimentally measured the performance and vibratory loads of a rotor with highly similar blades, then evaluated the predictive capability of the comprehensive analysis tool UMARC using the measured data. The following key conclusions are drawn:

1. Non-instrumented rotor blades were built in-house with no more than 2.5% variance in their structural and inertial properties, half of that of the instrumented set of blades built previously. Bending and torsional stiffnesses, natural frequencies, blade inertia, and mass distribution were successfully measured accurately for each blade.
2. Highly similar rotor blades and direct pitch measurements demonstrated improved rotor track and trim for advance ratios up to 0.7, evidenced by 30% lower peak-to-peak flapping than that of the instrumented blades. Sustained dissimilarities in the blades and an imbalance in the rotor and hub, were aggravated by the high advance ratio flow environment, resulted in the rotor being slightly out-of-track and 0.5° outside of the original trim target for $\mu > 0.7$.
3. Tests at higher rotor RPMs (40%-50% of nominal) demonstrated a maximum advancing tip Mach number ($M = 0.53$) closer to the design tip Mach number of 0.60, providing more meaningful performance and drag measurements.
4. The vibratory hub loads generally increase with advance ratio, and vertical out-of-plane forcing is a maximum at $\mu = 0.9$. The vertical hub loads show a dominant 4/rev component. A large 1/rev component in the in-plane forces indicates a mass imbalance in the rotor and hub, while the same feature in the normal force indicates an aerodynamic imbalance.
5. A comparison of performance measurements to predictive results demonstrates good overall agreement for advance ratios from 0.3 to 0.7. At high collectives, the thrust is slightly over-predicted and the power is somewhat under-predicted, while the rotor lift-to-drag ratio is satisfactorily predicted. Thrust reversal is shown to occur at $\mu = 0.9$ for this rotor in both experimental and predicted results. This agrees with the advance ratios at which reversal occurs in the literature ($0.8 > \mu > 1.0$).
6. The effects of longitudinal shaft tilt ($\pm 4^\circ$) were studied for advance ratios of 0.5, 0.7, and 0.8. Rotor lift-to-drag ratio increased significantly for lower collectives at high μ (+10% at $\theta_0 = 0^\circ$ and $\mu = 0.8$) simply by adding 4° of rearward shaft tilt. UMARC analyses correlate well with zero and aft shaft tilt, but underestimate power and overestimate thrust, resulting in a slight over-prediction of lift-to-drag ratio.
7. Limited cases were run with and without a simplified fuselage to characterize the effects on the rotor, and results indicate the fuselage induces no significant change in performance for $\mu < 0.7$. Lateral cyclic was affected by the fuselage at high μ , and the increased slope of θ_{IC} versus θ_0 was likely the result of upwash over the front portion of the rotor disk.

FUTURE WORK

Future tests will focus on further refining the vibratory loads measurements of the UMD rotor and test stand. A new dynamic calibration of the test stand will be performed in the wind tunnel to understand the frequency and vibratory response of the rotor test stand mounted on the wind tunnel balance as well as its effects on the vibratory loads measurements. Additional testing will also investigate the aeromechanics of a more realistic compound rotorcraft configuration, systematically investigating the interactions of wings and propellers on the rotor and fuselage. CFD modeling will contribute to the understanding of the flow environment over and around the rotor, hub, and fuselage.

ACKNOWLEDGEMENTS

This experimental work was supported by the Army/Navy/NASA Vertical Lift Research Center of Excellence (VLRCoE), led by Dr. Mahendra J. Bhagwat, Program Manager and Technical Agent, under Cooperative Agreement number W911W6-17-2-0004. The predicted results and validation with test data were supported by the Israel Ministry of Defense with Dr. Tal Yehoshua as a Technical Monitor and Dr. Omri Rand (Technion) as a Research Advisor. Wind tunnel testing was carried out alongside Dr. Anya Jones and Dr. Andrew Lind, whose PIV results are described in detail in the ERF 2017 paper by Lind et al., "Flowfield Measurements of Reverse Flow on a High Advance Ratio Rotor". The authors thank the staff of the Glenn L. Martin Wind Tunnel as well as fellow researchers Dr. Vikram Hrishikeshavan, Peter

Oas, and Jon Detoro for their assistance with rotor blade fabrication, fuselage design, and wind tunnel testing.

REFERENCES

- [1] DARPA, "Broad Agency Announcement: Vertical Take-off and Landing Experimental Plane (VTOL X-Plane)," DARPA-BAA-13-19, February, 2013.
- [2] J. B. Wheatley and M. J. Hood, "Full-Scale Wind Tunnel Tests of the PCA-2 Autogiro Rotor," Langley Aeronautical Laboratory, NACA Report No. 515, January, 1935.
- [3] J. L. Jenkins, "Wind-Tunnel Investigation of a Lifting Rotor Operating at Tip-Speed Ratios from 0.65 to 1.45," NASA Langley Research Center, NASA-TN-D-2628, February, 1965.
- [4] J. C. Biggers, R. H. Stroub and J. L. McCloud III, "An Investigation of Full Scale Helicopter Rotors at High Advance Ratios and Advancing Tip Mach Numbers," NASA Ames Research Center, NASA-TN-D-4632, July, 1968.
- [5] B. Charles and W. Tanner, "Wind Tunnel Investigation of Semirigid Full-Scale Rotors Operating at High Advance Ratios," Bell Helicopter, Report 576-099-010, January, 1969.
- [6] F. D. Harris, "Rotor Performance at High Advance Ratio: Theory versus Test," NASA Ames Research Center, NASA/CR-2008-215370, 2008.
- [7] M. Floros and W. Johnson, "Stability and Control Analysis of the Slowed-Rotor Compound Helicopter," *Journal of the American Helicopter Society*, vol. 52, no. 3, pp. 239-253, 2007.
- [8] R. Ormiston, "Rotor Aerodynamic Characteristics at High Advance Ratios Relevant to Compound Rotorcraft," in American Helicopter Society Future Vertical Lift Aircraft Design Conference, San Francisco, CA, January, 2012.
- [9] A. Datta, H. Yeo and T. R. Norman, "Experimental Investigation and Fundamental Understanding of a Full-Scale Slowed Rotor at High Advance Ratios," *Journal of the American Helicopter Society*, vol. 58, no. 2, pp. 1-17, 2013.
- [10] M. Potsdam, A. Datta and B. Jayaraman, "Computational Investigation and Fundamental Understanding of a Slowed UH-60A Rotor at High Advance Ratios," *Journal of the American Helicopter Society*, vol. 61, no. 2, pp. 1-17, 2016.
- [11] X. Wang, A. Saxena and I. Chopra, "Measurement and Validation of a Mach-Scale Rotor Performance and Loads at High Advance Ratios," in Proceedings of the 72nd Annual Forum of the American Helicopter Society, West Palm Beach, FL, May, 2016.
- [12] B. Berry and I. Chopra, "Slowed Rotor Wind Tunnel Testing of an Instrumented Rotor at High Advance Ratio," in 40th European Rotorcraft Forum, Southampton, UK, September, 2014.
- [13] B. Berry and I. Chopra, "Wind Tunnel Testing of an Instrumented Rotor at High Advance Ratio," in 56th AIAA Structures, Structural Dynamics, and Materials Conference, Kissimmee, FL, January, 2015.
- [14] G. Bowen-Davies and I. Chopra, "Aeromechanics of a Slowed Rotor," *Journal of the American Helicopter Society*, vol. 60, no. 3, pp. 1-13, 2015.
- [15] G. Bowen-Davies and I. Chopra, "Performance and Loads Correlation of the UH-60 Rotor at High Advance Ratios," in 40th European Rotorcraft Forum, Southampton, England, September 2014.
- [16] I. Chopra and G. Bir, "University of Maryland Advanced Code: UMARC," in American Helicopter Society Aeromechanics Specialists Conference, San Francisco, CA, January 1994.
- [17] D. H. Hodges and E. H. Dowell, "Nonlinear Equations of Motion for the Elastic Bending and Torsion of Twisted Nonuniform Rotor Blades," NASA Ames Research Center, NASA TP-1566/AVRADCOM TR 80-A-1, 1980.
- [18] A. Bagai and J. G. Leishman, "Rotor Free-Wake Modeling Using a Relaxation Technique - Including Comparisons with Experimental Data," *Journal of the American Helicopter Society*, vol. 40, no. 2, 1995.
- [19] J. G. Leishman, "Validation of Approximate Indicial Aerodynamic Functions for Two-Dimensional Subsonic Flow," *Journal of Aircraft*, vol. 25, no. 10, pp. 914-922, 1988.
- [20] J. G. Leishman and T. S. Beddoes, "A Semi-Empirical Model for Dynamic Stall," *Journal of the*

American Helicopter Society, vol. 34, no. 3, pp. 3-17, 1989.

COPYRIGHT STATEMENT

The author(s) confirm that they, and/or their company or organization, hold copyright on all of the original material included in this paper. The authors also confirm that they have obtained permission, from the copyright holder of any third party material included in this paper, to publish it as part of their paper. The authors confirm that they give permission, or have obtained permission from the copyright holder of this paper, for the publication and distribution of this paper as part of the ERF2017 proceedings or as individual offprints from the proceedings and for inclusion in a freely accessible web-based repository.